



BN_{0.5}O_{0.4}C_{0.1}: Carbon- and oxygen-substituted hexagonal BN

L.A.J. Garvie^{a,*}, H. Hubert^b, P. Rez^b, P.F. McMillan^{b,c}, P.R. Buseck^{a,c}

^aDepartment of Geology, Arizona State University, Tempe, AZ 85287-1404, USA

^bCenter for Solid State Science, Arizona State University, Tempe, AZ 85287-1704, USA

^cDepartment of Chemistry and Biochemistry, Arizona State University, Tempe, AZ 85287-1604, USA

Received 24 September 1998

Abstract

Hexagonal boron nitride (hex BN) containing significant amounts of C and O substituting for N (hex BCNO) was synthesized at 75 kbar and 1700°C from mixtures of C, B₂O₃, and amorphous B contained in a hex BN crucible. Hex BCNO is a minor constituent of the product and occurs as small, <30 nm diameter, rounded pseudo-hexagonal particles adhering to materials with the α -rhombohedral B structure. Electron energy-loss spectroscopy with a transmission electron microscope was used to quantify their elemental ratios. Up to 50% of the N in hex BN is replaced by C and O, e.g., BN_{0.49}O_{0.38}C_{0.11}. The electron energy-loss near-edge fine structure of the core-loss edges was used to elucidate the possible structures of hex BCNO. The core-loss edges of B, C, N, and O exhibit orientation-dependent intensity changes, which indicates that they occupy similar anisotropic bonding sites in graphite-like BCNO layers. For a composition of BN_{0.5}O_{0.4}C_{0.1}, regions with B–N₃, B–N₂O, and B–NO₂ units predominate. In addition, some grains have significant quantities of B–O₃ and B–C₃ units. Boron–boron bonding is either absent or infrequent. © 1999 Elsevier Science S.A. All rights reserved.

Keywords: Electron energy-loss spectroscopy; Boron nitride; Solid solution; High pressure; High temperature

1. Introduction

Materials with compositions intermediate between graphite and hexagonal BN (hex BN) are attractive because of the possibility of synthesizing materials with electronic properties intermediate between conducting (semi-metallic) graphite and insulating hex BN. For example, addition of N or B dopants to graphite or to diamond alters their electronic structure and changes their band gaps and the carrier concentrations. Intermediate C-hex BN compounds are thought to be good starting materials for the preparation of cubic BCN materials with high hardness [1–4]. Several intermediate graphitic materials in the BCN system have been produced by CVD and chemical reaction of B-, C-, and N-bearing derivatives [5–12] and by high-pressure and/or temperature methods [13–15]. Several studies have shown evidence of extensive solid solutions of graphite-like B–C–N materials [16,17], although graphite-like B–N–O solid solutions are unknown. The compound “B₂O” has been reported as the result of high pressure synthesis, and has been proposed to have either a

layered (“graphitic”) or ordered diamond-like structure [18,19]. However, recent results from our group cast doubt on the identity of the material obtained by those synthetic routes, and indicate that the stable boron suboxide phase is in fact B₆O_{1– δ} ($\delta=0.75–0.96$), with an icosahedral structure based on α -rhombohedral boron (α -rh. B) [20–23].

Analysis of materials in the B–C–N system is commonly hampered by difficulties of sample identification and characterization. For example, it is difficult to distinguish between a nanometer-scale mixture of graphite and hex BN and a substitutional ternary network with most diffraction or spectroscopic methods [24]. Several spectroscopic methods provide information on the compositions and structures of light-element-bearing materials such as x-ray photoelectron (XPS), x-ray emission (XES), and electron energy-loss spectroscopy (EELS). XPS spectra provide chemical and bonding information, although at low spatial resolutions. Chemical information at high spatial resolution can be gained by EELS with a transmission electron microscope (TEM). EELS is well adapted to light-element analysis [20,25–28]. The spatial resolution is governed by the probe size in the TEM, which can be as small as 3 Å in a dedicated scanning TEM (STEM), although the actual probe size used is dictated by the electron-beam sensitivity of the sample and counting statistics.

*Corresponding author. Tel.: +1-480-965-7250; fax: +1-480-965-8102.

E-mail address: lgarvie@asu.edu (L.A.J. Garvie)

Inherent in the EELS spectrum is information on the environment of the excited atom such as bonding, oxidation state, coordination, and site symmetry [25–27,29–34]. An EELS spectrum displays electron intensity as a function of the energy lost by electrons as they pass through a specimen [35]. Core-loss edges result from the transitions of core electrons to unoccupied states in the conduction band and probe the unoccupied density of states (UDOS). Close to the edge onset and for small scattering vectors, the transitions that give rise to the core-loss edge are governed by the atomic dipole selection rules for electronic transitions $\Delta l = \pm 1$, and $\Delta j = 0, \pm 1$, where l and j are the orbital and total angular momentum quantum numbers of the excited electron's subshell. The edge shape within ca. 40 eV of the edge onset, the energy-loss near-edge structure (ELNES), reflects the projection of the atom-resolved, partial density of unoccupied states of the conduction band. Alignment of core-loss spectra on a common energy scale allows similarities between the ELNES of different atoms to be related to mixing of local conduction-band states. For example, core-loss edges of Mn oxides [30], borates and borides [20,27,28], sulfides [36], and SrTiO₃ [33] exhibit similarities among their ELNES features, which gives insight into the nature of the unoccupied states.

In the course of our research program on high-pressure, high-temperature syntheses of boron-rich materials in the B–C–N–O system, we produced small quantities of a new crystalline phase based on hex BN, containing significant quantities of C and O, as a byproduct in some runs. Here we report on the quantification and determination of the structure of this material by TEM and EELS.

2. Experimental

Samples were synthesized with a Walker-type multianvil apparatus [37]. The pressure medium consisted of an MgO octahedron, and force was applied by eight WC cubes with corners truncated to triangular faces. Amorphous B (99.999%), B₂O₃ (99.99%), and C (99.999%) were mixed in proportions according to $16 B + xC + yB_2O_3$, with $x = 2$ or 4 and $y = 1$ or 3. The primary aim of these experiments was to synthesize materials with the α -rh. B structure [21–23,28]. The mixtures were pressed into a pellet and enclosed in a hex BN capsule. The encapsulated material was then placed in a graphite resistance furnace, pressurized to 7.5 GPa, and heated at 1700°C for 30 minutes to 5 hours. Temperature inside the cell was calibrated with a W–5%Re/W–25%Re thermocouple.

Small pieces of the reactants were crushed with a boron carbide pestle and mortar in methanol. A drop of the finely divided material in suspension was then dried on a lacy-C film supported on a Cu TEM grid. Lacy-C films were used so that data could be recorded from thin electron-beam-transparent grains protruding over the holes. To reduce

carbon contamination in the TEM, the TEM grid supporting the finely crushed material was placed on a 100 Watt light bulb for ~10 minutes just prior to insertion in the TEM. A thermocouple placed on the bulb gave a reading of ~170°C. Failure to place the sample on the bulb invariably resulted in the buildup of carbonaceous material during the recording of PEELS data, which was a problem since the C K edge from the contamination interfered with the C K edge from the materials under investigation.

Spectra were acquired with a Gatan 666 parallel EELS [38] spectrometer attached to a Philips 400-ST FEG TEM operated at an accelerating voltage of 100 keV in cold-cathode mode. The width of the zero-loss peak at half height was 0.7 eV. Spectra were acquired with convergence and collection angles of 16 and 11 mrad, respectively. The probe current was 10 to 15 nA, and spectra were acquired from regions ca. 20 nm diameter. Core-loss edges were obtained from thin areas, typically <50 nm thick, overhanging holes in the lacy C film. Spectra for near-edge structure studies were acquired with a dispersion of 0.1 eV/channel and a 1 or 2 s acquisition time. At least five spectra were acquired for each edge and each spectrum shifted by ~0.5 eV. The resulting set of data were then aligned and summed. For quantitative analysis, spectra were acquired with a dispersion of 1 eV, acquisition time of 2 s, and a thermally-assisted FEG. All spectra were acquired in diffraction mode from areas of approximately 20 nm diameter. The dark current and a background of the form AR^{-7} was subtracted from beneath each core-loss edge. The high-resolution K edges were further processed by deconvoluting the effects of the asymmetry of the zero-loss peak and the point-spread function following the procedures of Egerton [35]. The PEELS spectra were analyzed with the Gatan el/p PEELS software and the elemental ratios determined using Hartree-Slater cross sections.

3. Results

3.1. Products

The dominant run products have the α -rh. B structure, with compositions intermediate between B₄C and B₆O [21–23,28]. One sample contains numerous boron carbide nanorods. Up to several weight percent N are found in the B₄C–B₆O materials, derived from the hex BN capsule used to contain the reaction mixtures. Small round particles, up to 30 nm in diameter, adhere to the nanorods and B₄C–B₆O grains (Fig. 1). These particles exhibit B and N K core-loss edges, with shapes that are different from the α -rh. B-bearing materials. In addition to B and N, these particles also contain substantial C and O (see below), and are termed here “hex BCNO”. Although the hex BCNO material was a frequent by-product in these runs, it constitutes a minute fraction of the reaction product and

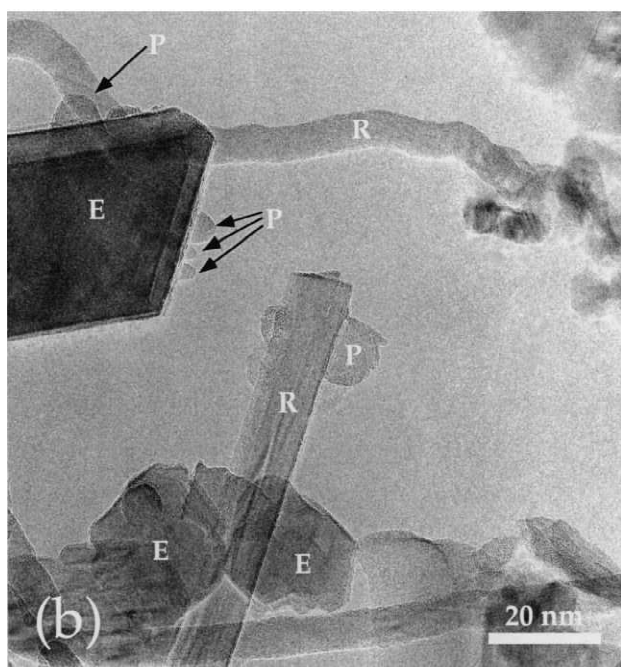
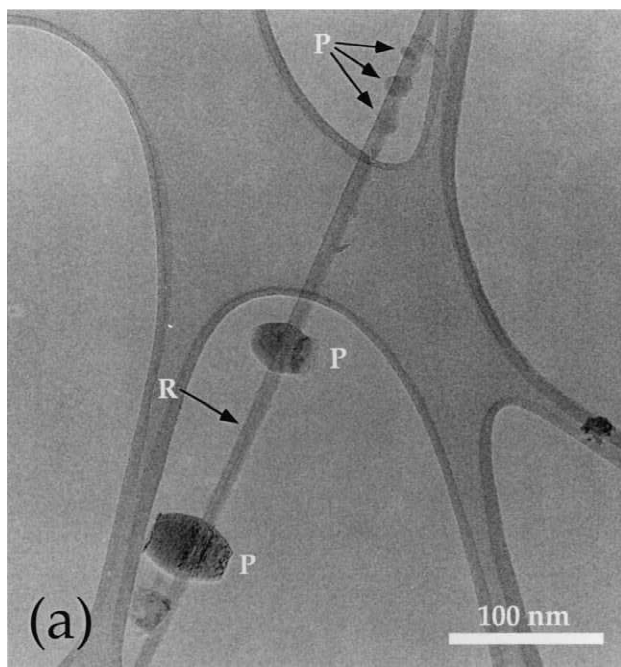


Fig. 1. TEM images of round hex BCNO particles (P) adhering to (a) a B_6C nanorod (R) and (b) euhedral B_4C – B_2O particles (E).

could not be separated for study by bulk analytical techniques. The TEM and EELS techniques are, however, ideally suited for structural and chemical characterization of this new phase.

3.2. Chemical analysis

A low-resolution EELS spectrum of hex BCNO (Fig. 2) shows an intense B K edge, a weaker N K edge, and small C and O K edges. Quantitative analyses give B:N ratios

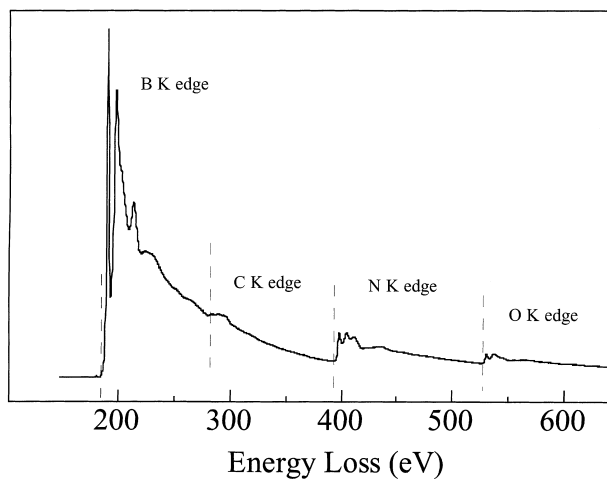


Fig. 2. Low-resolution EELS spectrum of a typical hex BCNO particle. The AE^{-r} background was subtracted from beneath the B K edge. The dotted vertical lines indicate the edge onsets.

near 1:0.5 for all particles analyzed. Representative analyses are given in Table 1. Also shown in Table 1 are duplicate analyses, illustrating the precision of the EELS method when applied to such light-element analysis. Differences between duplicate analyses are less than $\pm 10\%$ for B, N, and O. Differences for C are frequently greater than $\pm 10\%$, because of the difficulty of accurately quantifying the weak C K edge, which rests on the slope of the intense B K edge extended fine structure. The average of four particles gives the chemical composition as $BN_{0.54}O_{0.36}C_{0.12}$ or $BX_{1.02}$. Thus, around half of the N atoms in stoichiometric BN are substituted by O and C, with an O:C ratio of approximately 3:1.

3.3. Core-loss edges and structure

The core-loss edges of hex BN and BCNO are compared in Fig. 3. The B and N K edges of hex BCNO and hex BN have similar shapes although the hex BCNO edges are broader (Fig. 4). The first peak on the B K edge of three-fold-coordinated B is attributed to transitions of the

Table 1

Representative analyses of four hex BCNO particles (1 to 4). Elemental ratios are normalized to boron. Duplicate analyses (a and b) are presented for each grain to illustrate the reproducibility of the quantification

Element	1a	1b	2a	2b	3a	3b	4a	4b
B	1.0	1.0	1.0	1.0	1.0	1.0	1.0	1.0
N	0.56	0.59	0.59	0.59	0.47	0.50	0.50	0.50
O	0.36	0.31	0.33	0.30	0.39	0.37	0.40	0.43
C	0.11	0.10	0.08	0.10	0.13	0.10	0.20	0.12

Average of grain a and

b.

1) $BN_{0.57}O_{0.33}C_{0.11}$

2) $BN_{0.59}O_{0.32}C_{0.09}$

3) $BN_{0.49}O_{0.38}C_{0.11}$

4) $BN_{0.50}O_{0.42}C_{0.15}$

Sum of N,O, and C compared to B.

$BX_{1.01}$

$BX_{1.00}$

$BX_{0.98}$

$BX_{0.97}$

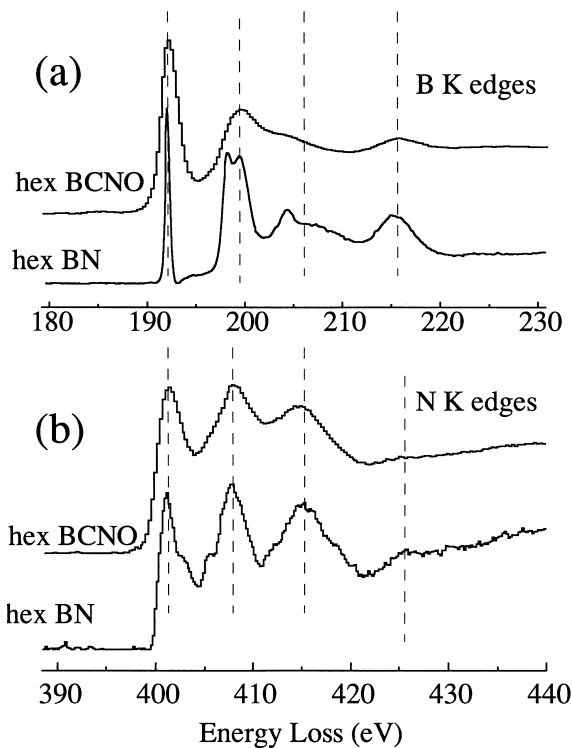


Fig. 3. Comparison of the B and N K edges of hex BCNO and hex BN. (a) B K edges and (b) N K edges. Dotted vertical lines illustrate the similarities between the ELNES of the two materials.

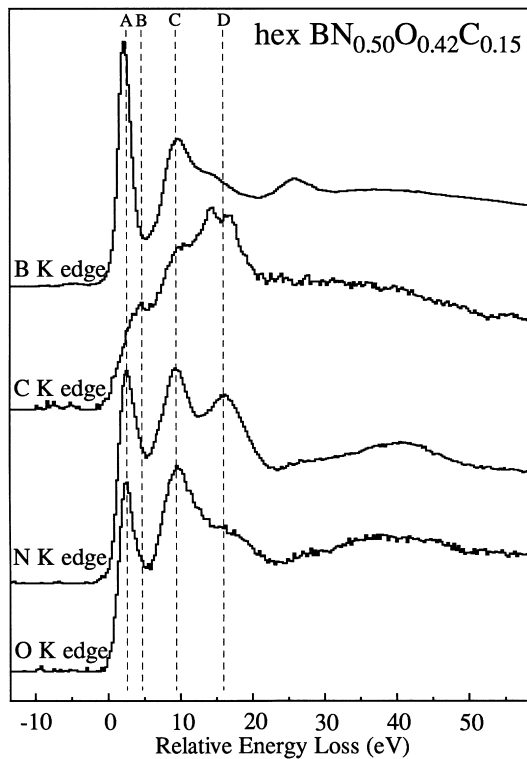


Fig. 4. Core-loss edges of hex BCNO. All spectra are plotted on a common energy scale and aligned relative to their ELNES and the conduction-band (CB) onsets. Features A through D are discussed in the text.

B 1s electron to states with π^* symmetry and is indicative of sp^2 bonding [27 and references therein]. The close similarities between the B and N K edges are indicative of strong covalent bonding between B and N. Likewise, the O and N K edge shapes are virtually identical, suggesting a similar bonding environment for each element (Fig. 4).

The shape of the C K edge differs from the other K edges (Fig. 4), but its features align with those of the other edges. The C K edge of hex BCNO has a different shape from those of graphite and amorphous C (Fig. 5), indicating that the C is not from a nanometer-scale mixture of hex B–N–O and elemental C. The C K edge has a similar shape to that of C in LiBC (Fig. 5), suggesting a similar environment for the C atoms in both materials. The structure of LiBC consists of alternating layers of Li and graphite-like BC [39], with each B surrounded by three C.

The π^* peaks of hex BCNO exhibit orientation-dependent intensity changes (Fig. 6). The concomitant orientation effects at all of the K edges indicate that B, C, N, and O occupy similar anisotropic bonding sites. With an electron probe parallel to the c -axis ($e^- \parallel c$ -axis) of hex BCNO, more excitations into states of σ character are detected than into states of π character, whereas a probe perpendicular to the c -axis ($e^- \perp c$ -axis) results in detection of similar numbers of excitations into states of each character, with resulting higher π^* peak intensity. Orientation dependence arises because of the directionality of the transitions to the unoccupied states into which the core electron is excited. In EELS, the scattering vector, \mathbf{q} , selects the direction probed within the crystal, and the direction of \mathbf{q} is determined by the differences between the wave vectors of the incident and the scattered high-energy electron. In our experiments the electron beam is focused into a probe with a half angle of convergence of 8 mrad, and the scattered electrons are collected over a cone of half

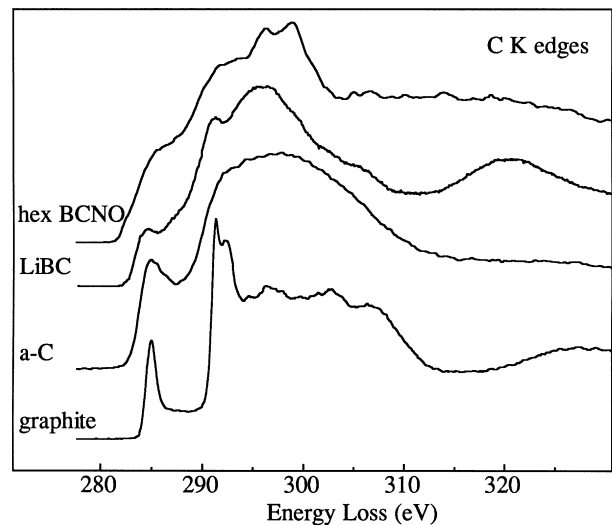


Fig. 5. C K edges of hex BCNO, LiBC, amorphous C (a-C), and graphite.

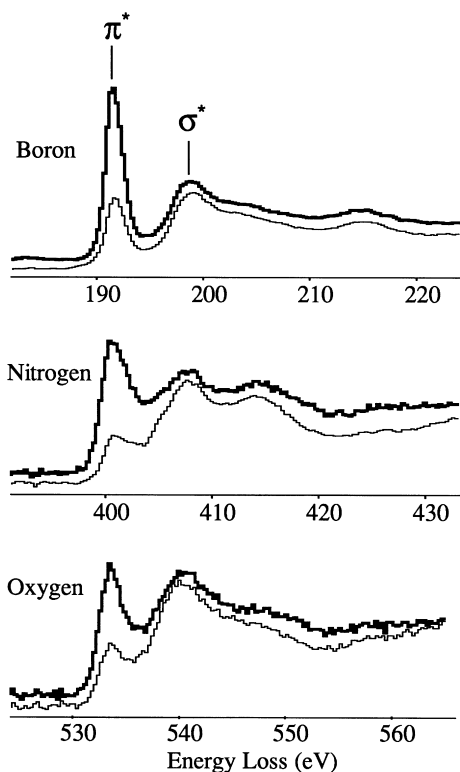


Fig. 6. B, N, and O K edges of hex BCNO, with the electron beam parallel (thin line) and perpendicular (thick line) to the c -axis. The spectra have been aligned vertically by the π^* peak and normalized to the intensity of the first σ^* peak.

angle of 5.5 mrad having a range of scattering angles that exceeds the characteristic angle of the inelastic scattering process, θ_E . Hence, scattering events over a wide range of \mathbf{q} vectors are collected, with those having \mathbf{q} perpendicular to the electron beam being dominant.

4. Discussion

The edge shapes, orientation dependences, and a formula close to $BX_{1.0}$ indicate that O and C substitute for N, within a presumed structure similar to hex BN. This is consistent with the observed grain morphology. Several different possibilities can be proposed for the graphite-like BCNO network, e.g., BN layers alternating with BO_xC_y layers; BX layers with X randomly one of C, N, and O; or BX layers with some ordered replacement of C, N, and O for X. The shape of the B K edge π^* peak gives an insight into these three possible structures.

For planar $B-X_3$ triangles, the π^* peak energies vary as a function of the electronegativity of X, e.g., B– B_3 in CrB_2 (188.8 eV), B– C_3 in LiBC (189.3), B– N_3 in hex BN (192.1 eV), B– O_3 in glassy B_2O_3 (194.1 eV), and B– F_3 in BF_3 (195.5 eV) (Fig. 7). The peak maximum of most π^* peaks of hex BCNO is at 192.1 eV, typical of B– N_3 bonding as in hex BN. The shoulder at 192.8 eV is

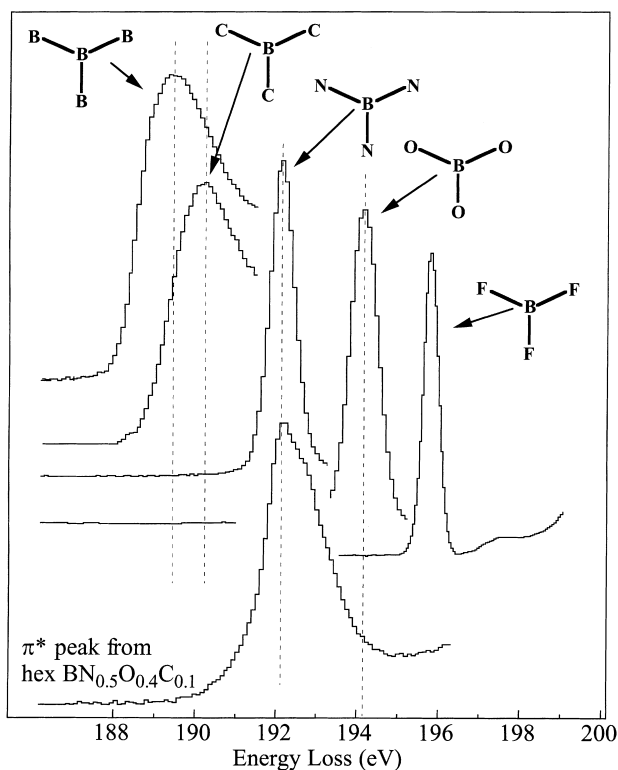


Fig. 7. Comparison of the B K π^* peaks of three-fold-coordinated B bonded to B (in CrB_2), C (in LiBC), N (in hex BN), O (in glassy B_2O_3), F (in BF_3 gas), and hex BCNO. The BF_3 spectrum from [41]. For clarity the spectra are offset vertically.

intermediate in energy between the B– N_3 and B– O_3 B K π^* peak maxima, possibly arising from B– NO_2 or B– N_2O triangles. Broad tails occur on both sides of the π^* peak; such tailing is not seen for the corresponding peak from hex BN. The tail on the low-energy side is presumably from B connected to C. A distinct B– C_3 π^* peak is not visible, which suggests that C randomly replaces N, with few distinct B– C_3 units. The high-energy tail indicates a range of B–OX units such as B–OCN and B– C_2O . The π^* peaks from different particles exhibit a range of shapes (Fig. 8), which reflect different proportions of the structural units, i.e., a degree of compositional heterogeneity. For example, in Fig. 8a, the B– N_2O peak is more intense than the B– N_3 peak, whereas the reverse is true for Fig. 8c. In addition, Fig. 8a has structures that represent B– C_3 , B– O_2N , and B– O_3 units.

Fig. 9 illustrates a possible atomic arrangement of hex BCNO with composition $BN_{0.5}O_{0.4}C_{0.1}$, with the assumption that there is minimal B–B and N–N bonding. Evidence of B–B and N–N bonding would have been visible as edge intensity below their respective K edge onsets. The shape of the B K edge π^* peak rules out a structure composed of alternating layers of BN and $BO_{0.8}C_{0.2}$. A layer with B:O:C elemental ratios of 5:4:1 would have a predominance of B– O_3 units that would give an intense π^* peak at ca. 194 eV, well separated from the B– N_3 π^*

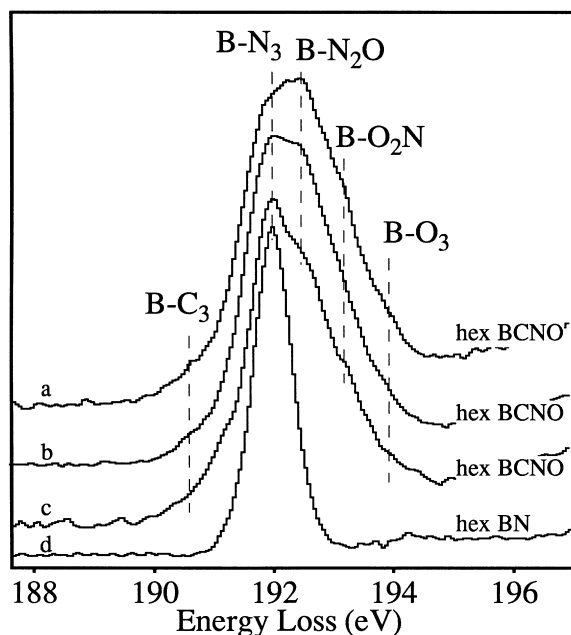


Fig. 8. Representative π^* peaks of different grains of hex BCNO (a, b, and c), and the π^* peak of hex BN (d). Prominent maxima or shoulders are marked with dashed vertical lines, and the structural units responsible for these peaks are shown.

peak; such a peak is not visible. With a ratio of B:N:O:C of 10:5:4:1, it is not possible to randomly replace N in stoichiometric hex BN with O and produce predominantly B-N₃, B-N₂O, and B-NO₂ units. In order to form these units, O and N must be segregated, as in Fig. 9, forming

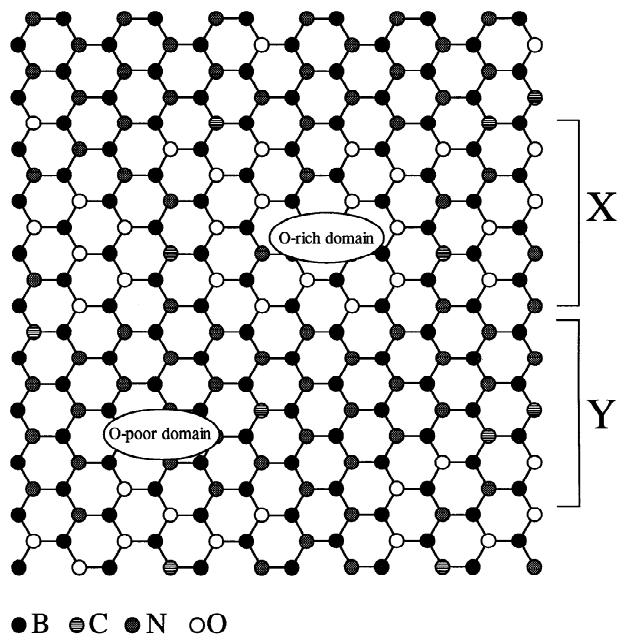


Fig. 9. Possible atomic arrangement of a layer of hex BCNO viewed down the *c*-axis with B:N:O:C ratio of 10:5:4:1. Each C, N, and O is surrounded by three B. The structural units B-N₃, B-N₂O, and B-NO₂ predominate, with fewer B-O₃, B-NOC, B-N₂C, B-C₂O, and B-O₂C units. Letters X and Y illustrate O- and N-rich domains, respectively.

regions with dominant B-N₃ units and domains rich in B-N₂O and B-NO₂ regions. The range of B K π^* peak shapes (Fig. 8) indicates that there are many different clusterings of structural units.

There has been much previous work on the synthesis and stability ranges of the hexagonal (graphitic) and cubic (zincblende structure) phases of boron nitride [40]. It has long been thought that the stable phase at atmospheric pressure is the graphitic phase, with the cubic BN (c-BN) stabilized at high pressure, above approximately 30 to 40 GPa at 1500 to 2000 K. This would be consistent with the phase relations between graphite and diamond within the carbon phase diagram. However, establishment of the equilibrium phase relations is impeded by the slow conversion kinetics between hex BN and c-BN, as in the carbon system, and much of the information has been from experimental results on ternary or more complex systems, or from experimental runs containing fluxes or catalytic impurities. The most recent results and compilation of previously published information on the BN system indicate that it is in fact the *cubic* phase that is thermodynamically stable at ambient pressure and temperature, and that the hex BN phase is stabilized only at high temperature [40]. Its ready synthesis at or near ambient pressure and at all temperatures can be attributed to kinetic considerations.

The hex BCNO phase obtained in the present study was formed as a minority phase along with cubic material of similar composition (this will be described in a forthcoming report), and with the nanorods and bulk particles of BCNO materials based on the α -rh. B structure [21]. It obviously did not form under equilibrium conditions, and these experiments do not allow us to place any constraints on its likely stability limits. This will be addressed in future work.

The analyzed composition of the hex BCNO material found in this study does not plot within the isoelectronic C-BN-B₂O ternary diagram: the analyzed composition (BN_{0.5}O_{0.4}C_{0.1}) is deficient in boron component (or, equivalently, too rich in O or N components). This finding indicates that the material has an excess of bonding electrons compared to the graphitic C-BN-B₂O solid solution, and hence could have interesting electronic properties. We are pursuing attempts to analyze the band structure of this material, and to obtain larger quantities in bulk form.

5. Conclusions

EELS in a TEM was essential for characterizing the hex BCNO material because it occurs as only <30 nm diameter rounded hexagonal platelets adhering to the α -rh B-rich grains and boron carbide nanorods. EELS is ideal for characterizing B-bearing materials since the K edges are well separated in energy, allowing easy determination

of the elemental ratios. In addition, the ELNES of the core-loss edges provides qualitative information on the bonding and local band structures.

The great advantage of EELS-TEM lies in its ability to quantify light elements at high spatial resolutions. EELS of nanometer-scale regions is becoming routine as more TEMs are fitted with EELS spectrometers. High-spatial resolution microanalysis is ideal for studying small precipitates and low-dimensional systems as well as materials that exist only at the microscopic scale.

Acknowledgements

This study was supported by the grants from the National Science Foundation, EAR-9219376 and MRSEC award DMR-96-32635. EELS spectra were acquired at the Center for High Resolution Electron Microscopy within the Center for Solid State Science at ASU.

References

- [1] A. Badzian, *Mat. Res. Bull.* 16 (1981) 1385.
- [2] E. Knittle, R.B. Kaner, R. Jeanloz, M.L. Cohen, *Phys. Rev. B* 51 (1995) 12149.
- [3] Y. Bando, S. Nakano, K. Kurashima, *J. Electron Microsc.* 45 (1996) 135.
- [4] T. Komatsu, M. Nomura, Y. Kakudate, S. Fujiwara, *J. Mater. Chem.* 6 (1996) 1799.
- [5] T.M. Besmann, *J. Am. Ceram. Soc.* 73 (1990) 2498.
- [6] L. Maya, L.A. Harris, *J. Am. Ceram. Soc.* 73 (1990) 1912.
- [7] F. Saugnac, F. Teyssandier, A. Marchand, *J. Am. Ceram. Soc.* 75 (1992) 161.
- [8] M. Kawaguchi, T. Kawashima, *J. Chem. Soc., Chem. Comm* (1993) 1133.
- [9] K. Nakamura, *Proc. 11th Int. Symp. Boron, Borides and Related Compounds*, Tsukuba, 1993, *JJAP Series* 10 (1994) 164.
- [10] L. Filipozzi, A. Derré, J. Conard, L. Piraux, A. Marchand, *Carbon* 33 (1995) 1747.
- [11] S. Flandrois, B. Ottaviani, A. Derre, A. Tressaud, *J. Phys. Chem. Solids* 57 (1996) 741.
- [12] M. Kawaguchi, T. Kawashima, T. Nakajima, *Chem. Mater.* 8 (1996) 1197.
- [13] T. Sekine, H. Kanda, Y. Bando, M. Yokoyama, K. Hojou, *J. Mat. Sci. Letts.* 9 (1990) 1376.
- [14] Yu.G. Andreev, T. Lundström, *J. Alloys Comp.* 210 (1994) 311.
- [15] E.Z. Kurmaev, A.V. Ezhov, S.N. Shamin, V.M. Cherkashenko, Yu.G. Andreev, T. Lundström, *J. Alloys Comp.* 248 (1997) 86.
- [16] A. Badzian, T. Badzian, *Int. J. of Refractory Metals and Hard Materials* 15 (1997) 3.
- [17] R.B. Kaner, J. Kouvetakis, C.E. Warble, M.L. Sattler, N. Bartlett, *Mat. Res. Bull.* 22 (1987) 399.
- [18] T. Endo, T. Sato, M. Shimada, *J. Mater. Sci. Lett.* 6 (1987) 683.
- [19] H.T. Hall, L.A. Compton, *Inorg. Chem.* 4 (1965) 1213.
- [20] L.A.J. Garvie, P. Rez, P.R. Buseck, *J. Solid State Chem.* 133 (1997) 347.
- [21] H. Hubert, L.A.J. Garvie, P.R. Buseck, W.T. Petuskey, P.F. McMillan, *J. Solid State Chem.* 133 (1997) 356.
- [22] H. Hubert, L.A.J. Garvie, D. Devouard, P.R. Buseck, W.T. Petuskey, P.F. McMillan, *Nature* 391 (1998) 376.
- [23] H. Hubert, L.A.J. Garvie, D. Devouard, P.R. Buseck, W.T. Petuskey, P.F. McMillan, *Chem. Materials* 10 (1998) 1530.
- [24] T. Lundström, Yu.G. Andreev, *Mat. Sci. Eng. A209* (1996) 16.
- [25] R. Brydson, H. Sauer, W. Engel, J.M. Thomas, E. Zeitler, *J. Chem. Soc., Chem. Comm.* 15 (1989) 1010.
- [26] R. Brydson, H. Sauer, W. Engel, E. Zeitler, *Microscopy, Microanalysis, Microstructures* 2 (1991) 159.
- [27] L.A.J. Garvie, R. Brydson, A.J. Craven, *Amer. Mineral.* 80 (1995) 1132.
- [28] L.A.J. Garvie, H. Hubert, P.R. Buseck, W.T. Petuskey, P.F. McMillan, *J. Solid State Chem.* 133 (1997) 365.
- [29] L.A.J. Garvie, A.J. Craven, R. Brydson, *Amer. Mineral.* 79 (1994) 411.
- [30] L.A.J. Garvie, A.J. Craven, *Phys. Chem. Minerals* 21 (1994) 191.
- [31] L.A.J. Garvie, P.R. Buseck, *Nature* 396 (1998) 667.
- [32] L.A.J. Garvie, P.R. Buseck, *Amer. Miner.* 84 (1998) 946.
- [33] T. Guerlin, H. Sauer, W. Engel, E. Zeitler, *Physica Status Solidi (a)* 150 (1995) 153.
- [34] P. Ildefonse, D. Cabaret, P. Sainctavit, G. Calas, A.M. Flank, P. Lagarde, *Phys. Chem. Minerals* 25 (1998) 112.
- [35] R.F. Egerton, in: *Electron Energy-Loss Spectroscopy in the Electron Microscope*, 2nd ed, Plenum Press, New York and London, 1996.
- [36] D. Li, G.M. Bancroft, M. Kasrai, M.E. Fleet, B.X. Yang, X.H. Feng, K. Tan, M. Peng, *Phys. Chem. Miner.* 20 (1994) 489.
- [37] K. Leinenweber, J. Parise, *J. Solid State Chem.* 114 (1985) 277.
- [38] O.L. Krivanek, C.C. Ahn, R.B. Keeney, *Ultramicroscopy* 22 (1987) 103.
- [39] M. Wörle, R. Nesper, G. Mair, M. Schwarz, H.G. Schnering, *Z. Anorg. Allg. Chem.* 621 (1995) 1153.
- [40] V.L. Solozhenko, *High Pressure Res.* 13 (1995) 1995.
- [41] E. Ishiguro, S. Iwata, Y. Suzuki, A. Mikuni, T. Sasaki, *J. Phys. B: Atomic Mol. Phys.* 15 (1982) 1841.